



Contents lists available at ScienceDirect

Journal of Quantitative Spectroscopy & Radiative Transfer

journal homepage: www.elsevier.com/locate/jqsrt

Temperature-dependent absorption cross-sections of HCFC-142b

Karine Le Bris^{a,*}, Kimberly Strong^b^a Department of Physics, Saint Francis Xavier University, P.O. Box 5000, Antigonish, NS, Canada B2G 2W5^b Department of Physics, University of Toronto, 60 St. George Street, Toronto, Ontario, Canada M5S 1A7

ARTICLE INFO

Article history:

Received 31 July 2009

Received in revised form

2 October 2009

Accepted 7 October 2009

Keywords:

Hydrochlorofluorocarbons

R-142b

Cross-sections

Mid-infrared

FTIR

Gas phase

Density functional theory

Vibrational wave number

Band strength

ABSTRACT

Following the recent detection of HCFC-142b (1-chloro-1,1-difluoroethane) from space, laboratory infrared absorption cross-section spectra of this molecule in a pure vapour phase have been recorded in the 650–3500 cm⁻¹ spectral region using Fourier transform spectroscopy. The spectra have been recorded at a resolution of 0.02 cm⁻¹ and a range of temperatures from 223 to 283 K. The resulting data show good agreement with the harmonic frequencies and intensities calculated using density functional theory as well as with the integrated absorption intensities of the spectral bands available in the literature. The new cross-sections will allow more accurate retrieval of atmospheric HCFC-142b concentrations using infrared spectroscopic techniques.

© 2009 Elsevier Ltd. All rights reserved.

1. Introduction

Hydrochlorofluorocarbons (HCFCs) are temporary substitutes for chlorofluorocarbons (CFCs). They were introduced after the phase-out of the latter by the Montreal Protocol and its subsequent amendments. Unlike CFCs, which are mainly destroyed by solar ultraviolet radiation in the stratosphere, the HCFCs, which contain one or more hydrogen atoms, can react with OH radicals in the troposphere to create HF and CO₂. Therefore, as less chlorine is transported to the stratosphere, the ozone depletion potentials of HCFCs are substantially weaker than those of CFCs. However, because of their C–Cl and C–F bonds, these molecules still have large absorption cross-sections in the atmospheric window region (8–12 μm), which give them strong global warming potentials.

HCFC-142b (1-chloro-1,1-difluoroethane) is a colourless gas at ambient pressure. It is mainly used as a chemical intermediate to produce fluoropolymers, as a blowing agent for expanded polystyrene and as a component of refrigerant fluids. Because of its high vapour pressure and low vapour solubility, HCFC-142b partitions mostly into the atmosphere. Today, this is the third most abundant hydrochlorofluorocarbon after HCFC-22 and HCFC141-b. The atmospheric lifetime of HCFC-142b is 17.9 years ±24% [1]. Its ozone depletion potential has been estimated at 0.07 while its global warming potential is evaluated to be 2310 ±810 for a horizon of 100 years [1].

The volume mixing ratio of HCFC-142b has been rising steadily in the atmosphere since the beginning of the 1990s, exceeding 20 ppt in 2008 at 13–16 km with an average positive trend of more than 5% per year [2]. The atmospheric concentration of HCFC-142b is now high enough to allow its detection from space [2,3]. However, the accuracy of the retrieval is limited by the lack of spectroscopic knowledge of this molecule. Only three cross-section spectra corresponding to the temperatures

* Corresponding author. Tel.: +1 902 867 2392; fax: +1 902 867 2414.
E-mail address: klebris@stfx.ca (K. Le Bris).

253, 270 and 287 K are currently available in the HITRAN 2008 database [4]. Measurements of temperature-dependent infrared cross-sections of HCFC-142b vapour at low temperature were reported in the 1990s [5–7] but discrepancies exist between these studies. No new laboratory data at low temperature have been published on this molecule since 1995.

As a result, uncertainties on the spectroscopic parameters of HCFC-142b are seen as one of the main sources of error for atmospheric retrievals [3]. New laboratory measurements are therefore crucial to enable accurate observations of the spatial and temporal variation of this hydrochlorofluorocarbon in the atmosphere.

The purpose of this study is to provide new infrared (IR) cross-sections of HCFC-142b at relatively high resolution (0.02 cm^{-1}) and at a range of relevant atmospheric temperatures (from 223 to 283 K). The resulting experimental data are compared to theoretical calculations performed using density functional theory and to previously published values.

2. Experimental setup

Experimental data are obtained using Fourier transform infrared (FTIR) absorption spectroscopy. The Fourier transform spectrometer (FTS) is a Bomem DA8.002 equipped with a KBr beamsplitter and operating with a Globar source.

The gas sample (SynQuest Labs, purity >98%) is contained in a stainless steel cell positioned between the FTS and a liquid nitrogen-cooled mercury cadmium telluride (MCT) detector. A vacuum system equipped with a Varian Turbo-V V250 turbo molecular pump allows the cell to be evacuated to about 1×10^{-6} Torr. The cell pressure is measured using 10 and 1000 Torr MKS baratron pressure gauges simultaneously.

HCFC-142b presents very intense lines in the atmospheric window region. In order to avoid saturation effects while working at relevant pressures, a stainless steel cell with an optical path of 3.17 cm was constructed. ZnSe windows were sealed to the cell with indium O-rings to prevent leakage at low temperature. The windows are maintained in place by stainless steel flanges supporting teflon rings.

The cooling is achieved by a Neslab ULT-80 chiller sending the coolant (Syltherm XLT) to a copper tube surrounding the cell. The copper tube is soldered to the cell and covered by thermally conductive epoxy to provide temperature homogeneity. The cell temperature is measured by a thermocouple directly inserted inside the cell. The temperature readout accuracy during experiments is typically $\pm 0.1^\circ\text{C}$.

Many sources of errors and artefacts can affect an FTIR spectrum, such as spectral aliasing, dynamic alignment error, blackbody emission from the source aperture, non-linearity of the MCT detector in the mid-infrared, etc. The r.m.s. angular deviation from optimum alignment is less than 10^{-6} rad in normal laboratory conditions (data provided by the manufacturer).

The blackbody emission from the source aperture comes from the warming of the iris by the light source. The warm annulus around the aperture acts as a second infrared source emitting off-axis thermal radiation. This leads to distortion of the signal shape and intensities as the aperture size decreases. To reduce this warm aperture artefact, a second iris is inserted between the DA8 spectrometer and the MCT detector at the focal point of the beam [8]. After this installation, no variation of the cross-section signal with the aperture size has been observed.

The non-linearity of the MCT detector, corresponding to the non-linearity between the measured signal and the photon flux, essentially affects the central fringe of the interferogram, which leads to a zero-level offset in the absorption spectrum. Correction of non-linearity is applied on the raw interferograms before the phase correction and the Fourier transformation. We adjusted the response of the detector to the light intensity by a curve whose only unknown parameter is an empirically chosen DC output value [9]. This parameter is adjusted by a minimization of the transmission in the spectral region below the cut-off wave number. The residual baseline offset is subtracted from the spectra after phase correction and Fourier transformation.

3. Data analysis

For each temperature, a series of spectra were recorded at a minimum of six different pressures between 2 and 12 Torr. Each pressure–temperature (P – T) spectrum is composed of at least 200 unapodised scans. The resulting spectrum, for each temperature, is a composite spectrum from the P – T spectrum sets extrapolated to the zero-Torr limit. A 200-scan primary baseline spectrum with an empty cell was recorded at each temperature. Secondary control baselines of at least 20 scans were also taken before and after each sample measurement to account for the small intensity variations that can occur during the long periods (typically several hours) of acquisitions. If necessary, the primary baseline is adjusted to the secondary baselines by a polynomial regression prior to the division of each sample spectrum by the adjusted baseline spectrum.

The cross-section, $\sigma(\nu)$, in $\text{cm}^2/\text{molecule}$ is calculated for each P – T set using the well-known Beer–Lambert law:

$$I(\nu) = I_0(\nu) e^{-\chi(\nu)} \quad (1)$$

with optical depth:

$$\chi(\nu) = \sigma(\nu) \frac{PT_0}{TP_0} N_L L \quad (2)$$

where ν is the wave number (cm^{-1}); $I_0(\nu)$, the light intensity passing through the empty cell (baseline); $I(\nu)$, the light intensity passing through the sample gas cell; N_L is the Loschmidt's constant (2.6868×10^{19} molecules/ cm^3); L , the length of the cell (cm); and P_0 and T_0 , the standard conditions for pressure and temperature.

To prevent saturation effects in an optically thick medium while keeping a good signal-to-noise ratio at every wave number, the points corresponding to optically thick ($\chi(\nu) > 1.1$) or optically thin ($\chi(\nu) < 0.1$) conditions are

eliminated. This way, a linear behaviour is obtained for strong absorption bands from the low-pressure measurements while the weak absorption features are represented by the high-pressure measurements.

The shapes of the ro-vibrational transition lines, as well as the peaks of the *Q*-branches, are pressure-dependent due to collisional broadening. The cross-section for each wave number is obtained at the zero-Torr limit by the linear least-square fit of the experimental apparent cross-section of the remaining values ($0.1 < \chi(\nu) < 1.1$) versus the pressure.

The errors on optical path length, temperature readout, pressure, baseline drift, and sample purity have been evaluated to account for less than $\pm 3\%$. The other sources of error in spectral measurements come from the residual MCT non-linearity, a possible residual baseline drift and the errors induced by the data reduction. For each wave number, we calculated the standard deviation σ between the linear fit and the apparent cross-section values as a function of pressure. The error for each wave number is chosen at the 95% confidence limit (2σ).

4. Results

HCFC-142b is a near-prolate asymmetric top molecule belonging to the C_s symmetry group (Fig. 1). As a consequence, it has 18 fundamental vibration modes (11 with A'

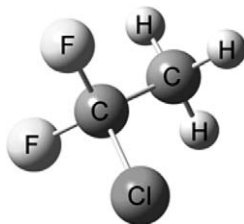


Fig. 1. Geometrical structure of HCFC-142b.

symmetry and 7 with A'' symmetry). Twelve of those fundamental modes have active absorption bands in the spectral window region between 650 and 3500 cm^{-1} .

All the bands present a sharp *Q*-branch surrounded by less intense *P*- and *R*-branch structures (Fig. 2). No significant variation of the integrated band strength with temperature has been observed from 223 to 283 K for any of the bands (Fig. 3). Therefore, we can confirm that the superimposed hot bands and combination bands of HCFC-142b do not alter the total integrated band intensities of strong fundamental modes in our range of temperatures.

The shape of the bands is strongly dependent on the temperature. The *Q*-branches become sharper as the temperature decreases due to the change of relative populations of the rotational states of the vibrational bands. This leads to a significant increase in the cross-sections at the band centers with decreasing temperature (Fig. 4).

The uncertainty on the integrated band strength is stable with temperature for all bands with the exception of the ν_8 band. The increased uncertainty on the integrated strength of the ν_8 band as the temperature decreases is likely due to the intense sharpening of the ν_8 *Q*-branch which worsens the data reduction error on the main peak.

Weak features of magnitude lower than $10^{-20} \text{ cm}^2/\text{molecule}$, which can be attributed either to overtones and combination band or sample impurity, are present at all temperatures in the spectral region between 1500 and 2800 cm^{-1} .

5. Data validation

5.1. Comparison with theoretical calculation of vibrational modes and intensities

The unconstrained geometric optimizations and harmonic vibrational frequencies of HCFC-142b are calculated using density functional theory (DFT) with Gaussian 03 [10].

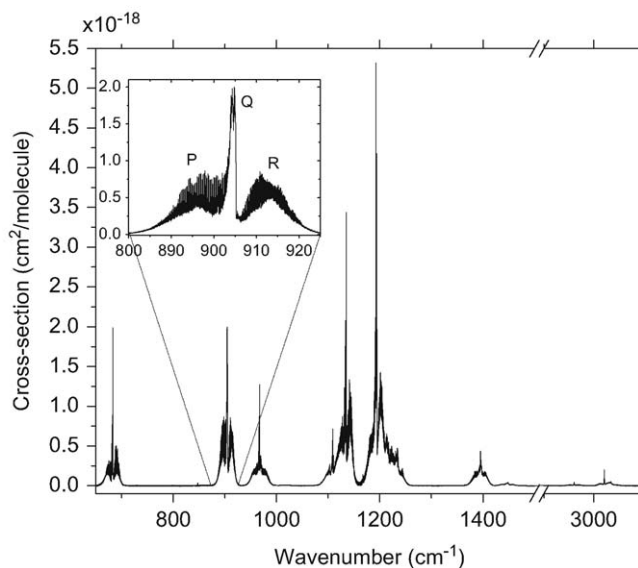


Fig. 2. Survey spectrum of HCFC-142b in the mid-infrared at 263 K.

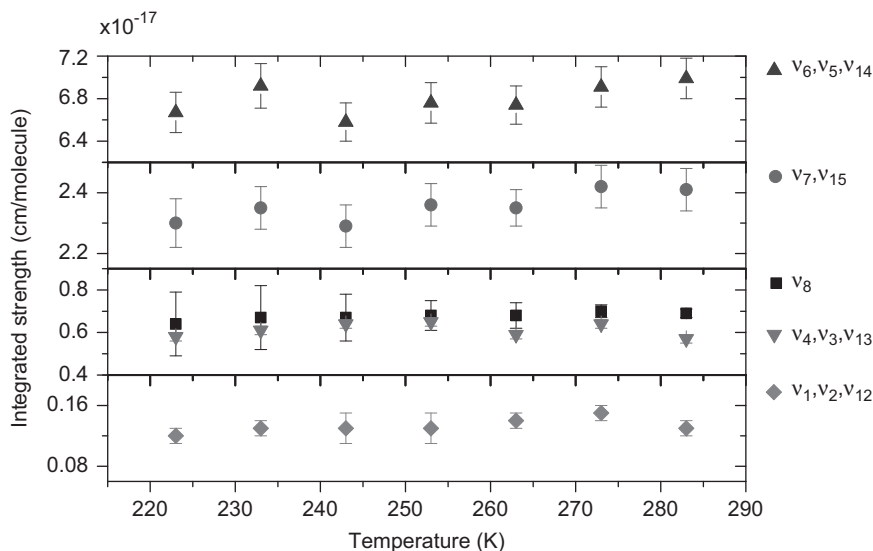


Fig. 3. Variation of the integrated strength of the five main absorption bands of HCFC-142b in the mid-infrared.

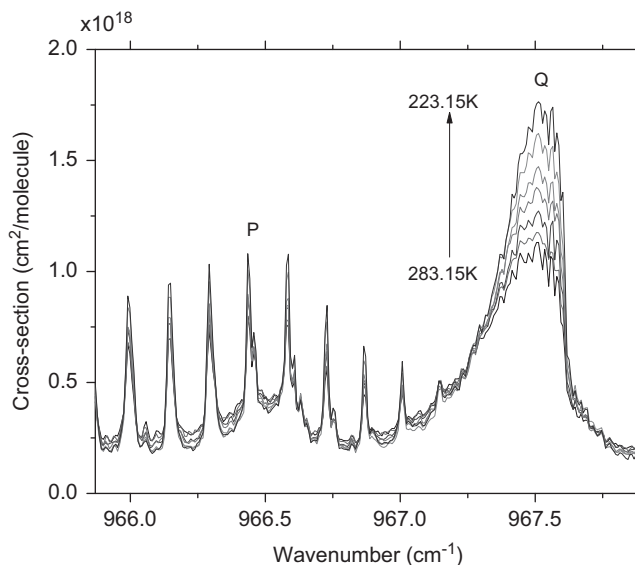


Fig. 4. Cross-section of the P- and Q-branches of the ν_{15} band of HCFC-142b at seven different temperatures.

Previous ab initio calculations for HCFC-142b have been carried out at the RHF/6-31* [11] and MP2/6-31G** [12] levels. The present DFT calculations are performed using the Becke's three-parameter functionals for the exchange and the Lee–Yang–Parr and Perdew–Wang non-local functionals for correlation (respectively, B3LYP and B3PW91). For each functional set, two basis sets are used: the Pople's type valence triple-zeta basis supplemented by multiple polarization and diffuse functions (6-311++(3df,3pd)) and the augmented correlation-consistent polarized quadruple-zeta (aug-cc-pVQZ) basis.

We observe a very good agreement between the geometries from the four levels of theory. The choice of the correlation functionals and the size of the basis sets have only a weak influence on the geometry. The

harmonic wave number positions present little sensitivity to basis sets, with an average difference below 0.2%, and to the correlation functionals, with an average difference around 0.7%. The variations of intensity with basis sets are also weak in both cases, with the exception of the ν_{10} band, corresponding to C–Cl stretching. It may be noted that the inclusion of diffuse functions on hydrogen atoms has almost no influence on the geometry and harmonic frequencies of HCFC-142b. However, the choice of correlation functionals does have a strong influence on the intensities, with an average difference between LYP and PW91 above 12% and a maximum difference between 25% and 30% for the ν_4 and ν_{15} bands. Comparison with experimental data is therefore essential to test the validity of the methods.

Table 1

Theoretical harmonic wave numbers and intensities of the fundamental modes of HCFC-142b.

Label	Assignment	Wave number				Band strength			
		B3LYP		B3PW91		B3LYP		B3PW91	
		(a)	(b)	(a)	(b)	(a)	(b)	(a)	(b)
<i>A'</i>									
ν_1	CH ₃ sym. st.	3141.36	3136.41	3157.78	3152.34	0.06	0.06	0.05	0.05
ν_2	CH ₃ sym. st.	3063.13	3059.54	3071.15	3066.82	0.03	0.03	0.03	0.03
ν_3	CH ₃ sym. def.	1483.52	1483.83	1474.41	1474.57	0.01	0.01	0.01	0.01
ν_4	CH ₃ sym. def.	1421.65	1422.37	1412.26	1412.58	0.46	0.47	0.62	0.63
ν_5	CF ₂ sym. st., C–C st.	1217.65	1216.27	1231.51	1229.66	2.00	1.99	1.93	1.94
ν_6	C–Cl st., CF ₂ sym. def.	1129.57	1129.39	1128.24	1127.67	2.72	2.67	3.01	2.95
ν_7	CF ₂ sym. st.	892.16	889.67	903.03	900.49	2.10	2.14	1.83	1.88
ν_8	C–C–Cl def.	669.26	668.25	678.87	677.57	0.98	0.98	0.94	0.94
ν_9	CF ₂ scissor	538.74	538.32	543.53	543.01	0.22	0.22	0.21	0.21
ν_{10}	C–Cl st.	424.24	421.51	431.71	428.52	0.05	0.05	0.04	0.04
ν_{11}	CClF ₂ –CH ₃ rock	301.07	299.86	301.40	299.99	0.02	0.02	0.02	0.02
<i>A''</i>									
ν_{12}	CH ₂ asym. st.	3157.99	3153.42	3173.96	3169.17	0.03	0.03	0.02	0.02
ν_{13}	CH ₃ asym. def	1480.50	1480.27	1471.51	1470.95	0.06	0.06	0.06	0.06
ν_{14}	CF ₂ asym. st.	1185.37	1183.27	1194.77	1192.94	2.36	2.33	2.64	2.61
ν_{15}	CF ₂ asym. st.	963.01	961.31	968.74	967.87	1.20	1.2	0.93	0.97
ν_{16}	CF ₂ rock	430.36	429.96	431.12	430.89	0.00	0.00	0.00	0.00
ν_{17}	CClF ₂ –CH ₃ twist	330.49	329.79	332.15	331.29	0.01	0.01	0.01	0.01
ν_{18}	Torsion	236.96	235.49	239.07	238.32	0.00	0.00	0.00	0.00

Wave numbers are in cm^{-1} , bands strengths are in 10^{-17} $\text{cm}^2/\text{molecule}$. (a) 6–311++ and (b) Aug-cc-pvqz. st:stretch, def: deformation.

Table 1 presents the assignment, the calculated harmonic wave number and the integrated strength of the fundamentals modes. The strongest bands correspond to C–C, C–Cl and C–F stretching vibrations. All of them fall in the $800\text{--}1250\text{ cm}^{-1}$ atmospheric window region, which explains the high global warming potential of this molecule.

The weak fundamental C–H stretching vibrations fall in the 3000 cm^{-1} spectral region. The superimposed CH₃ deformation vibrations lie in the 1400 cm^{-1} region. Only the ν_4 mode presents a medium intensity in this window.

The theoretical values of the harmonic frequencies have been compared to the experimental data (Fig. 5). The experimental line center is chosen at the barycentre of the Q-band. All four levels of theory give excellent results after an average linear scaling: $\nu_{\text{exp}} = (1.06 \pm 0.01)\nu_{\text{theo}} - (59.3 \pm 7.7)$, with ν_{exp} and ν_{theo} , the respective experimental and theoretical harmonic wave number values in cm^{-1} . The theoretical values for line intensity in the mid-IR spectral windows also fit relatively well the data after linear scaling with the experimental integrated absorption strength (see Fig. 6). We obtained an average $I_{\text{exp}} = (1.01 \pm 0.05)I_{\text{theo}} + (0.22 \pm 0.14) \times 10^{-17}$ for B3LYP and $I_{\text{exp}} = (1.10 \pm 0.02)I_{\text{theo}} + (0.08 \pm 0.05) \times 10^{-17}$ for B3PW91, with I_{exp} and I_{theo} the respective experimental and theoretical integrated band strengths in $\text{cm}^2/\text{molecule}$. However, B3PW91 gives the best correlation with an R^2 of 0.999 for both basis sets.

5.2. Comparison with published values

The integrated band intensities of the HCFC-142b cross-section spectra are compared with data available

in the literature (Table 2). The integrated intensities of the four absorption bands ν_8 , (ν_7 , ν_{15}), (ν_6 , ν_5 , ν_{14}), and (ν_4 , ν_3 , ν_{13}) between 650 and 1500 cm^{-1} are reported. No previous values for the ν_1 , ν_2 , ν_{12} bands around 3000 cm^{-1} have been found in literature. At most temperatures, our integrated absorption band strengths show good agreement with earlier measurements for a pure vapour [5,6] as well as for N₂-broadened vapour [7,13]. No constant relative difference is observed with any of the data sets, which indicates that there were no significant systematic errors in the measurements.

The largest discrepancies between authors appears at 233 K. A disparity close to 20% for the ν_6 , ν_5 , ν_{14} absorption bands exists between Newnham and Ballard [5] and Cappellani and Restelli [7]. As previously mentioned, our integrated band strengths do not exhibit trends and our values at 233 K, midway between the values of these two studies, remain consistent with our results at other temperatures.

6. Conclusions

Absorption cross-sections of HCFC-142b at a spectral resolution of 0.02 cm^{-1} have been recorded in the mid-infrared between 650 and 3500 cm^{-1} at seven different temperatures (223, 233, 243, 253, 263, 273, and 283 K). The main sources of errors in the measurements have been investigated and accounted for in the final results. The integrated intensities of the harmonic wave number bands show good agreement with the data available in the literature and with theoretical calculations using DFT. The availability of cross-section spectra at 10-K steps between 223 and 283 K should, therefore, allow the reduction of

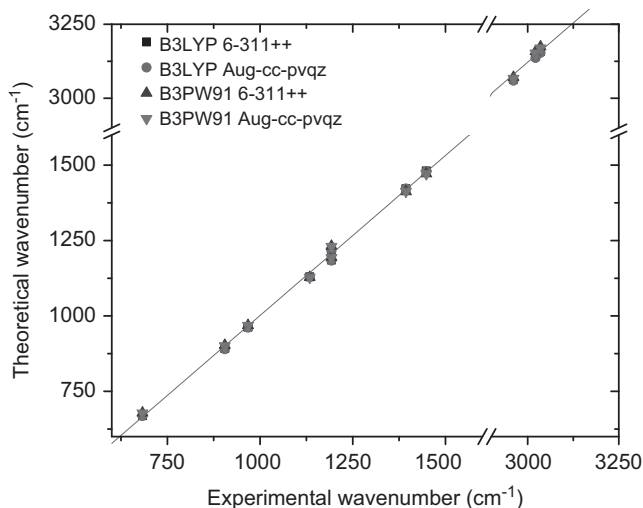


Fig. 5. Comparison between experimental and theoretical harmonic frequencies of HCFC-142b for the four levels of theory.

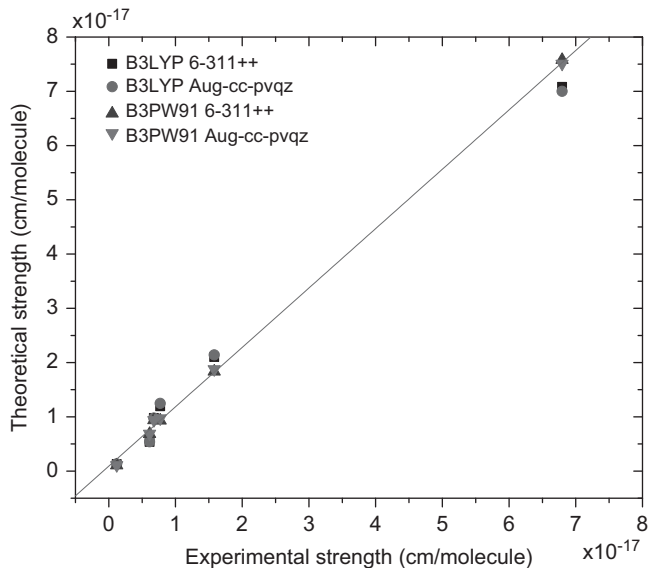


Fig. 6. Comparison between experimental and theoretical band strengths of HCFC-142b for the four levels of theory.

Table 2

Comparison of the experimental infrared integrated band strengths ($\times 10^{-17}$ cm/molecule) with published values when available.

Temperature	Label	Integrated band strength				
		This work	Ref. [13] ^a	Ref. [5] ^b	Ref. [6] ^c	Ref. [7]
293 K	ν_8		0.74	0.71 ± 0.01		0.74
	ν_7, ν_{15}		2.53	2.49 ± 0.07		2.38
	ν_6, ν_5, ν_{14}		7.06	7.34 ± 0.10		6.94
	ν_4, ν_3, ν_{13}		0.64	0.58 ± 0.04		0.60
283 K	ν_8	0.69 ± 0.02			0.75 ± 0.05	
	ν_7, ν_{15}	2.41 ± 0.07			2.58 ± 0.14	
	ν_6, ν_5, ν_{14}	6.99 ± 0.19			7.19 ± 0.20	
	ν_4, ν_3, ν_{13}	0.57 ± 0.02			0.61 ± 0.09	
	ν_2, ν_1, ν_{12}	0.13 ± 0.01				
273 K	ν_8	0.70 ± 0.03	0.74	0.70 ± 0.04	0.69 ± 0.05	0.75
	ν_7, ν_{15}	2.42 ± 0.07	2.50	2.56 ± 0.07	2.51 ± 0.14	2.45

Table 2 (continued)

Temperature	Label	Integrated band strength				
		This work	Ref. [13] ^a	Ref. [5] ^b	Ref. [6] ^c	Ref. [7]
	ν_6, ν_5, ν_{14}	6.91 ± 0.19	7.05	7.06 ± 0.13	7.11 ± 0.20	7.12
	ν_4, ν_3, ν_{13}	0.64 ± 0.02	0.63	0.61 ± 0.03	0.64 ± 0.09	0.62
	ν_2, ν_1, ν_{12}	0.15 ± 0.01				
263 K	ν_8	0.68 ± 0.06				
	ν_7, ν_{15}	2.35 ± 0.06				
	ν_6, ν_5, ν_{14}	6.74 ± 0.18				
	ν_4, ν_3, ν_{13}	0.59 ± 0.02				
	ν_2, ν_1, ν_{12}	0.14 ± 0.01				
253 K	ν_8	0.68 ± 0.07		0.69 ± 0.03	0.68 ± 0.05	
	ν_7, ν_{15}	2.36 ± 0.07		2.41 ± 0.08	2.40 ± 0.14	
	ν_6, ν_5, ν_{14}	6.76 ± 0.19		6.16 ± 0.43	6.96 ± 0.20	
	ν_4, ν_3, ν_{13}	0.65 ± 0.02		0.65 ± 0.05	0.78 ± 0.09	
	ν_2, ν_1, ν_{12}	0.13 ± 0.02				
243 K	ν_8	0.67 ± 0.11				
	ν_7, ν_{15}	2.29 ± 0.07				
	ν_6, ν_5, ν_{14}	6.58 ± 0.18				
	ν_4, ν_3, ν_{13}	0.64 ± 0.02				
	ν_2, ν_1, ν_{12}	0.13 ± 0.02				
233 K	ν_8	0.67 ± 0.15		0.71 ± 0.01		0.75
	ν_7, ν_{15}	2.35 ± 0.07		2.30 ± 0.04		2.51
	ν_6, ν_5, ν_{14}	6.92 ± 0.21		6.19 ± 0.02		7.38
	ν_4, ν_3, ν_{13}	0.61 ± 0.02		0.62 ± 0.05		0.64
	ν_2, ν_1, ν_{12}	0.13 ± 0.01				
223 K	ν_8	0.64 ± 0.15				
	ν_7, ν_{15}	2.30 ± 0.08				
	ν_6, ν_5, ν_{14}	6.67 ± 0.19				
	ν_4, ν_3, ν_{13}	0.58 ± 0.02				
	ν_2, ν_1, ν_{12}	0.12 ± 0.01				
213 K	ν_8			0.70 ± 0.07		
	ν_7, ν_{15}			2.46 ± 0.05		
	ν_6, ν_5, ν_{14}			6.80 ± 0.28		
	ν_4, ν_3, ν_{13}			0.60 ± 0.04		
203 K	ν_8			0.79 ± 0.09		
	ν_7, ν_{15}			2.34 ± 0.26		
	ν_6, ν_5, ν_{14}			6.90 ± 0.10		
	ν_4, ν_3, ν_{13}			0.58 ± 0.03		

^a The first two temperature sets for Ref. [13] are at 297 and 277 K.

^b The first temperature set for Ref. [5] is at 296 K.

^c The first two temperature sets for Ref. [6] are at 287 and 270 K.

uncertainties on HCFC-142b volume mixing ratio retrieval from space missions. The cross-sections are provided online in supplementary data files and are also available from the corresponding author.

Acknowledgements

This work was supported by the Canadian Space Agency (CSA) and the Natural Sciences and Engineering Research Council of Canada (NSERC). We thank Paul Chen for technical support, and Prof. James R. Drummond and the NSERC Industrial Research Chair in Atmospheric Remote Sounding from Space (sponsored by COMDEV, Bomem, Environment Canada, CSA, and NSERC) for the use of the Bomem DA8 Fourier transform spectrometer. We also thank Dr. Stella M.L. Melo from the CSA and Dr. Chris

Boone from the University of Waterloo for helpful discussions.

Appendix A. Supplementary data

Supplementary data associated with this article can be found in the online version at doi:10.1016/j.jqsrt.2000.10.005.

References

- [1] WMO (World Meteorological Organization). Scientific assessment of ozone depletion: 2006, Global Ozone Research and Monitoring Project-Report, No. 50, Geneva, Switzerland; 2007.
- [2] Rinsland CP, Chiou L, Boone C, Bernath P, Mahieu E. First measurements of the HCFC-142b trend from atmospheric chemistry experiment (ACE) solar occultation spectra. JQSRT 2009;110:2127–34.

- [3] Dufour G, Boone CD, Bernath F. First measurements of CFC-113 and HCFC-142b from space using ACE-FTS infrared spectra. *Geophys Res Lett* 2005;32:L15S09.
- [4] Rothman LS, Gordon IE, et al. The HITRAN 2008 molecular spectroscopic database. *JQSRT* 2009;110:533–72.
- [5] Newnham D, Ballard J. Fourier transform infrared spectroscopy of HCFC-142b vapour. *JQSRT* 1995;53:471–9.
- [6] Clerbaux C, Colin R, Simon PC, Granier C. Infrared cross sections and global warming potentials of 10 alternative hydrohalocarbons. *J Geophys Res* 1993;98:10491–7.
- [7] Capellani F, Restelli G. Infrared band strengths and the temperature-dependence of the hydrohalocarbons HFC-134a, HFC152a, HCFC-22, HCFC-123, and HCFC-142b. *Spectrochim Acta Part A* 1992;48:1127–1131.
- [8] Johnson TJ, Sams RL, Blake TA, Sharpe SW, Chu PM. Removing aperture-induced artifacts from Fourier transform infrared intensity values. *Appl Opt* 2002;41:2831–9.
- [9] Abrams C, Toon GC, Schindler RA. Practical example of the correction of Fourier-transform spectra for detector nonlinearity. *Appl Opt* 1994;33:6307–14.
- [10] Frisch MJ, et al. Gaussian 03, Revision C.02. Wallingford, CT: Gaussian, Inc.; 2004.
- [11] Paddison SJ, Chen Y, Tschuikow-Roux E. An ab initio study of the structures, barriers for internal rotation, vibrational frequencies, and thermodynamic functions of the hydrochlorofluorocarbon $\text{CH}_3\text{CF}_2\text{Cl}$ and the corresponding radical $\text{CH}_2\text{CF}_2\text{Cl}$. *Can J Chem* 1994;72:561–7.
- [12] Papasavva S, Illinger K, Kenny J. Molecular properties of CFC substitutes from ab initio calculations: CFCl_2CH_3 , CF_2ClCH_3 , CHCl_2CF_3 and CHFClCF_3 . *J Mol Struct Theochem* 1997;393:73–83.
- [13] Sharpe SW, Johnson TJ, Sams RL, Chu PM, Rhoderick GC, Johnson PA. Gas-phase databases for quantitative infrared spectroscopy. *Appl Spectrosc* 2004;58:1452–61.